Joint International Topical Meeting on Mathematics & Computation and Supercomputing in Nuclear Applications (M&C + SNA 2007)
Monterey, California, April 15-19, 2007, on CD-ROM, American Nuclear Society, LaGrange Park, IL (2007)

A NODAL EXPANSION METHOD FOR SOLVING THE MULTIGROUP SP_3 EQUATIONS IN THE REACTOR CODE DYN3D

C. Beckert and U. Grundmann
Forschungszentrum Dresden-Rossendorf
Institute of Safety Research
PO Box 51 01 19, D-01314
Dresden, Germany
C.Beckert@fzd.de; U.Grundmann@fzd.de

ABSTRACT

The core model DYN3D which has been developed for three-dimensional analyses of steady states and transients in thermal reactors with quadratic or hexagonal fuel assemblies is based on nodal methods for the solution of the two-group neutron diffusion equation. Loading cores with higher content of MOX fuel, the increase of the fuel cycle length and new types of reactors are challenging for these standard methods. A nodal expansion method for solving the equations of the simplified P_3 approximation (SP_3) of the multigroup transport equation was developed to improve the accuracy of the DYN3D code. In this paper, the method used in DYN3D-SP3 is described. It is applied for the pinwise calculation of a steady state of the OECD/NEA and U.S. NRC PWR MOX/UO_2 Core Transient Benchmark. The eigenvalue *keff*, assembly powers and the pin powers are computed. The results calculated with different approaches including diffusion theory are compared with the reference solution obtained from a heterogeneous transport calculation with the code DeCART. Different approaches of the diffusion coefficient used in the SP_3 equations are investigated. The SP_3 results obtained with the transport cross section of multigroup diffusion theory show the smallest deviations from the reference solution. These deviations are in the same order as the results of the code DORT, whereas the DORT and DYN3D calculations were carried out with the same library of group constants for homogenized pin cells.

Key Words: SP_3, nodal methods, neutron transport, neutron diffusion, multigroup

1. INTRODUCTION

Steady-state and transient simulations of light water reactor cores are performed with standard methods based on the solution of the two-group neutron diffusion equation with nodal methods and assembly-wise group constants generated with the help of cell codes. Improvements of the standard technique are required because the core is loaded with MOX fuel, the unload burnup of the assemblies is increased and new types of reactors are considered. It is expected that the neutron field has to be calculated with more energy groups, a neutron transport approximation higher than diffusion theory and subnodes in the assemblies.

The three-dimensional core model DYN3D is based on standard methods for quadratic and hexagonal fuel assemblies [1]. The code was extended to an arbitrary number of neutron energy groups. A nodal expansion method based on the SP_3 approximation of the multigroup transport equation is developed and implemented in DYN3D-SP3. It allows to describe the assemblies not only as whole but also with finer meshes up to the pin cell level. The method which was

developed for quadratic fuel assemblies is described in section 2. DYN3D-SP3 is applied for the calculation of a steady-state of the OECD/NEA and U.S. NRC PWR MOX/UO_2 Core Transient Benchmark [2] in section 3. Pinwise calculations were performed with the new method and also the diffusion approximation. The eigenvalue k_{eff}, assembly and pin powers are compared with the transport solutions of the codes DeCART and DORT. The DeCART calculation [3] that acts as reference solution was performed with the method of characteristics. Seubert et. al [4] generated a 16-group XS-library with pinwise homogenized cross sections with the cell code HELIOS 1.8 [5] for the DORT calculations. The DYN3D calculations were carried out with the same library. Compared to the DeCART-reference solution the accuracy of the DYN3D calculations is strongly influenced by the approximation of the SP_3 diffusion coefficient. Section 4 provides a brief conclusion and an outlook.

2. THEORY

The SP_3 equations presented in subsection 2.1 are solved by a nodal method which is shortly described in subsection 2.2. This method allows to calculate the assemblies in radial direction by a number of subnodes. Different approximations of the diffusion coefficient which occurs in the SP_3 method are discussed in section 2.3.

2.1. The Multigroup SP_3 Equations

The spherical harmonics (P_N) approximation of the multigroup neutron transport equation is obtained by expanding the angular dependence of the neutron flux in spherical harmonic functions up to the order N. This approximation leads in general three-dimensional geometries to $(N+1)^2$ and in one-dimensional geometry to $N+1$ unknowns for the flux moments. In one-dimensional geometry the system is divided in intervals with spatially constant cross sections. Within the interval n, the steady-state multigroup P_N equations have the form

$$\frac{l}{2l+1}\frac{d}{dx}\Phi^n_{l-1,g}(x)+\frac{l+1}{2l+1}\frac{d}{dx}\Phi^n_{l+1,g}(x)+\Sigma^n_{t,g}\Phi^n_{l,g}(x)=\sum_{g'=1}^{G}\Sigma^n_{s,l,g'\to g}\Phi^n_{l,g'}(x)+Q^n_{l,g}(x) \quad (1)$$

for $l=0, 1,\ldots,N$ and each energy group g $(g=1,\ldots,G)$ with the flux moments Φ_l. For $l=0$ and $l=N$ it is assumed $\Phi_{-1}=0$ and $\Phi_{N+1}=0$ respectively. $\Sigma_{t,g}$ is the macroscopic total cross section of group g and $\Sigma_{s,l,g'\to g}$ the l^{th} moment of the macroscopic cross section for neutrons scattered from the energy group g' to group g. Assuming an isotropic external source Q_{ex} the group source is given by

$$Q^n_{0,g}(x)=\frac{1}{k_{eff}}\chi^n_g\sum_{g'=1}^{G}\nu\Sigma^n_{f,g'}\Phi^n_{0,g'}(x)+Q^n_{ex,g}(x) \quad \text{and} \quad Q^n_{l,g}(x)=0 \qquad \textit{for} \qquad l>0, \quad (2)$$

where k_{eff} is the effective multiplication factor, χ_g the fission spectrum of group g and $\nu\Sigma_{f,g'}$ the macroscopic production cross section of group g'.

Considering the equations (1) up to the order $N = 3$ ($l = 0, 1, 2, 3$) four linear differential equations for the flux moments $\Phi_{l,g}(x)$ are obtained:

$$\begin{aligned}
\frac{d}{dx}\Phi^n_{1,g}(x) + \Sigma^n_{t,g}\Phi^n_{0,g}(x) &= \sum_{g'=1}^{G}\Sigma^n_{s,0,g'\to g}\Phi^n_{0,g'}(x) + Q^n_{0,g}(x),\\
\frac{1}{3}\frac{d}{dx}\Phi^n_{0,g}(x) + \frac{2}{3}\frac{d}{dx}\Phi^n_{2,g}(x) + \Sigma^n_{t,g}\Phi^n_{1,g}(x) &= \sum_{g'=1}^{G}\Sigma^n_{s,1,g'\to g}\Phi^n_{1,g'}(x),\\
\frac{2}{5}\frac{d}{dx}\Phi^n_{1,g}(x) + \frac{3}{5}\frac{d}{dx}\Phi^n_{3,g}(x) + \Sigma^n_{t,g}\Phi^n_{2,g}(x) &= \sum_{g'=1}^{G}\Sigma^n_{s,2,g'\to g}\Phi^n_{2,g'}(x),\\
\frac{3}{7}\frac{d}{dx}\Phi^n_{2,g}(x) + \Sigma^n_{t,g}\Phi^n_{3,g}(x) &= \sum_{g'=1}^{G}\Sigma^n_{s,3,g'\to g}\Phi^n_{3,g'}(x).
\end{aligned} \tag{3}$$

Brantley and Larsen [6] assume within their SP_3 approximation that there is no anisotropic group to group scattering, if the groups are different, i. e.

$$\Sigma^n_{s,l,g'\to g} = 0 \quad \text{for} \quad g' \neq g, \quad l = 1, 2, 3\,. \tag{4}$$

With these assumptions, the 2nd, 3rd and 4th equation of (3) include only flux moments of the group g and the 2nd and 4th equation yield for the odd flux moments

$$\Phi^n_{1,g}(x) = -\frac{1}{3\Sigma^n_{r,1,g}}\frac{d}{dx}\left[\Phi^n_{0,g}(x) + 2\Phi^n_{2,g}(x)\right] \qquad \text{and} \qquad \Phi^n_{3,g}(x) = -\frac{3}{7\Sigma^n_{r,3,g}}\frac{d}{dx}\Phi^n_{2,g}(x) \tag{5}$$

with the "removal" cross sections

$$\Sigma^n_{r,l,g} = \Sigma^n_{t,g} - \Sigma^n_{s,l,g\to g} \quad \text{for} \quad l = 0, 1, 2, 3\,. \tag{6}$$

Inserting (5) in the 1st and 3rd equation of (3) the four first-order differential equations can be replaced by the two second-order differential equations for the 0th and 2nd flux moments

$$\begin{aligned}
-D^n_{0,g}\frac{d^2}{dx^2}\left[\Phi^n_{0,g}(x) + 2\Phi^n_{2,g}(x)\right] + \Sigma^n_{r,0,g}\Phi^n_{0,g}(x) &= \sum_{g'=1,g'\neq g}^{G}\Sigma^n_{s,0,g'\to g}\Phi^n_{0,g'}(x) + Q^n_{0,g}(x),\\
-\frac{2}{5}D^n_{0,g}\frac{d^2}{dx^2}\left[\Phi^n_{0,g}(x) + 2\Phi^n_{2,g}(x)\right] - D^n_{2,g}\frac{d^2}{dx^2}\Phi^n_{2,g}(x) + \Sigma^n_{r,2,g}\Phi^n_{2,g}(x) &= 0,
\end{aligned} \tag{7}$$

with

$$D^n_{0,g} = \frac{1}{3\Sigma^n_{r,1,g}} \qquad \text{and} \qquad D^n_{2,g} = \frac{9}{35\Sigma^n_{r,3,g}}\,. \tag{8}$$

In 1960 Gelbard [7] imposed the SP_3 equations for general three-dimensional geometry by replacing the second derivatives in the one-group P_3 equations for one-dimensional geometry by

the Laplace operator. Applying this approach in (7) and rearranging terms yield the corresponding SP_3 equations of (7) for three-dimensional geometry:

$$\begin{aligned} &-D^n_{0,g}\nabla^2[\Phi^n_{0,g}(\boldsymbol{r})+2\Phi^n_{2,g}(\boldsymbol{r})]+\Sigma^n_{r,0,g}\Phi^n_{0,g}(\boldsymbol{r})=S^n_{0,g}(\boldsymbol{r}),\\ &-D^n_{2,g}\nabla^2\Phi^n_{2,g}(\boldsymbol{r})+\Sigma^n_{r,2,g}(\boldsymbol{r})\Phi^n_{2,g}(\boldsymbol{r})-\frac{2}{5}\Sigma^n_{r,0,g}\Phi^n_{0,g}(\boldsymbol{r})=-\frac{2}{5}S^n_{0,g}(\boldsymbol{r}), \end{aligned} \tag{9}$$

with

$$S^n_{0,g}(\boldsymbol{r})=\sum_{g'=1,g'\neq g}^{G}\Sigma^n_{s,0,g'\to g}\Phi^n_{0,g'}(\boldsymbol{r})+\frac{\chi^n_g}{k_{eff}}\sum_{g'=1}^{G}\nu\Sigma^n_{f,g'}\Phi^n_{0,g'}(\boldsymbol{r})\,. \tag{10}$$

Now, the superscript n indicates three-dimensional volumes (nodes) with spatially constant cross sections. With the introduction of the unknowns

$$\hat{\Phi}^n_{0,g}(\boldsymbol{r})=\Phi^n_{0,g}(\boldsymbol{r})+2\Phi^n_{2,g}(\boldsymbol{r}) \qquad \text{and} \qquad \hat{\Phi}^n_{2,g}(\boldsymbol{r})=\Phi^n_{2,g}(\boldsymbol{r}) \tag{11}$$

the SP_3 equations (9) have the form

$$\begin{aligned} &-D^n_{0,g}\nabla^2\hat{\Phi}^n_{0,g}(\boldsymbol{r})+\Sigma^n_{r,0,g}\hat{\Phi}^n_{0,g}(\boldsymbol{r})-2\Sigma^n_{r,0,g}\hat{\Phi}^n_{2,g}(\boldsymbol{r})=S^n_{0,g}(\boldsymbol{r}),\\ &-D^n_{2,g}\nabla^2\hat{\Phi}^n_{2,g}(\boldsymbol{r})+\left[\Sigma^n_{r,2,g}+\frac{4}{5}\Sigma^n_{r,0,g}\right]\hat{\Phi}^n_{2,g}(\boldsymbol{r})-\frac{2}{5}\Sigma^n_{r,0,g}\hat{\Phi}^n_{0,g}(\boldsymbol{r})=-\frac{2}{5}S^n_{0,g}(\boldsymbol{r}). \end{aligned} \tag{12}$$

Brantley and Larsen's variational derivation of the SP_3 equations provides in addition to the equations (12) the interface and Marshak-like boundary conditions [6]. At the interface $\boldsymbol{r}_{ij}$ between the two volumes i and j the following conditions are obtained

$$\hat{\Phi}^i_{m,g}(\boldsymbol{r}_{ij})=\hat{\Phi}^j_{m,g}(\boldsymbol{r}_{ij}) \quad \text{and} \quad \boldsymbol{n}_i\boldsymbol{J}^i_{m,g}(\boldsymbol{r}_{ij})=\boldsymbol{n}_i\boldsymbol{J}^j_{m,g}(\boldsymbol{r}_{ij}) \tag{13}$$

with

$$\boldsymbol{J}^i_{m,g}(\boldsymbol{r})=-D^i_{m,g}\nabla\hat{\Phi}^i_{m,g}(\boldsymbol{r}) \quad \text{for} \quad m=0,2. \tag{14}$$

$\boldsymbol{n}_i$ is the unit outer normal vector of material zone i. The incoming (–) and outgoing (+) "partial currents" at any surface $\boldsymbol{r}_{ij}$ of a volume are given by

$$\begin{aligned} J^{\pm}_{0,g}(\boldsymbol{r}_{ij})&=\frac{1}{4}\hat{\Phi}^i_{0,g}(\boldsymbol{r}_{ij})\pm\frac{1}{2}\boldsymbol{n}_i\boldsymbol{J}^i_{0,g}(\boldsymbol{r}_{ij})-\frac{3}{16}\hat{\Phi}^i_{2,g}(\boldsymbol{r}_{ij}),\\ J^{\pm}_{2,g}(\boldsymbol{r}_{ij})&=-\frac{3}{80}\hat{\Phi}^i_{0,g}(\boldsymbol{r}_{ij})\pm\frac{1}{2}\boldsymbol{n}_i\boldsymbol{J}^i_{2,g}(\boldsymbol{r}_{ij})+\frac{21}{80}\hat{\Phi}^i_{2,g}(\boldsymbol{r}_{ij}). \end{aligned} \tag{15}$$

If there is vacuum at any outer surface $\boldsymbol{r}_{out}$ of the system, the boundary conditions are given by

$$J^-_{m,g}(\boldsymbol{r}_{out})=0, \quad m=0,2\,. \tag{16}$$

2.2. A Nodal Expansion Method for Solving the Multigroup SP_3 Equations

In the three-dimensional core calculations within the nodes, intranodal flux expansions by using polynomials and exponential functions are applied. In the following, functions of the radial plane (x, y) and of the axial direction z are not differently indicated to simplify the expressions. Transverse integration is carried out firstly in axial direction *z* over the node height a_z^n to reduce the equations (12) to two-dimensional equations in the radial plane

$$\begin{aligned} &-D_{0,g}^n\left(\frac{\partial^2}{\partial x^2}+\frac{\partial^2}{\partial y^2}\right)\hat{\Phi}_{0,g}^n(x,y)+\Sigma_{r,0,g}^n\hat{\Phi}_{0,g}^n(x,y)-2\Sigma_{r,0,g}^n\hat{\Phi}_{2,g}^n(x,y)=\hat{S}_{0,g}^n(x,y)-L_{0,g}^{tr,n}(x,y),\\ &-D_{2,g}^n\left(\frac{\partial^2}{\partial x^2}+\frac{\partial^2}{\partial y^2}\right)\hat{\Phi}_{2,g}^n(x,y)+\left[\Sigma_{r,2,g}^n+\frac{4}{5}\Sigma_{r,0,g}^n\right]\hat{\Phi}_{2,g}^n(x,y)-\frac{2}{5}\Sigma_{r,0,g}^n\hat{\Phi}_{0,g}^n(x,y)\\ &\qquad\qquad=-\frac{2}{5}\hat{S}_{0,g}^n(x,y)-L_{2,g}^{tr,n}(x,y), \end{aligned} \tag{17}$$

with

$$\hat{S}_{0,g}^n(x,y)=\sum_{g'=1,g'\neq g}^{G}\Sigma_{s,0,g'\to g}^n\left[\hat{\Phi}_{0,g'}^n(x,y)-2\hat{\Phi}_{2,g'}^n(x,y)\right]+\frac{\chi_g^n}{k_{eff}}\sum_{g'=1}^{G}\nu\Sigma_{f,g'}^n\left[\hat{\Phi}_{0,g'}^n(x,y)-2\hat{\Phi}_{2,g'}^n(x,y)\right], \tag{18}$$

and secondly in the *x*-*y* plane over the square node area (side length *a*) to reduce (12) to one-dimensional equations in *z*-direction

$$\begin{aligned} &-D_{0,g}^n\frac{\partial^2}{\partial z^2}\hat{\Phi}_{0,g}^n(z)+\Sigma_{r,0,g}^n\hat{\Phi}_{0,g}^n(z)-2\Sigma_{r,0,g}^n\hat{\Phi}_{2,g}^n(z)=\hat{S}_{0,g}^n(z)-L_{0,g}^{tr,n}(z),\\ &-D_{2,g}^n\frac{\partial^2}{\partial z^2}\hat{\Phi}_{2,g}^n(z)+\left[\Sigma_{r,2,g}^n+\frac{4}{5}\Sigma_{r,0,g}^n\right]\hat{\Phi}_{2,g}^n(z)-\frac{2}{5}\Sigma_{r,0,g}^n\hat{\Phi}_{0,g}^n(z)=-\frac{2}{5}\hat{S}_{0,g}^n(z)-L_{2,g}^{tr,n}(z), \end{aligned} \tag{19}$$

with

$$\hat{S}_{0,g}^n(z)=\sum_{g'=1,g'\neq g}^{G}\Sigma_{s,0,g'\to g}^n\left[\hat{\Phi}_{0,g'}^n(z)-2\hat{\Phi}_{2,g'}^n(z)\right]+\frac{\chi_g^n}{k_{eff}}\sum_{g'=1}^{G}\nu\Sigma_{f,g'}^n\left[\hat{\Phi}_{0,g'}^n(z)-2\hat{\Phi}_{2,g'}^n(z)\right], \tag{20}$$

where the equation systems (17) and (19) are coupled by the transversal leakages

$$L_{m,g}^{tr,n}(x,y)=-\frac{D_{m,g}^n}{a_z^n}\int_{-\frac{a_z^n}{2}}^{\frac{a_z^n}{2}}\frac{\partial^2}{\partial z^2}\tilde{\Phi}_{m,g}^n(x,y,z)\,dz,\quad m=0,2, \tag{21}$$

$$L_{m,g}^{tr,n}(z)=-\frac{D_{m,g}^n}{a^2}\int_{-\frac{a}{2}}^{\frac{a}{2}}\int_{-\frac{a}{2}}^{\frac{a}{2}}\left(\frac{\partial^2}{\partial x^2}+\frac{\partial^2}{\partial y^2}\right)\tilde{\Phi}_{m,g}^n(x,y,z)\,dxdy,\quad m=0,2. \tag{22}$$

Henceforth, the indices for the group *g* and the node *n* are omitted in this subsection. Inside the nodes the flux moments of each energy group are expanded

$$\hat{\Phi}_m(x,y) \approx c_{m,0}h_0 + \sum_{i=1}^{2} c_{m,i}^{x} h_i\left(\frac{x}{a}\right) + \sum_{i=1}^{2} c_{m,i}^{y} h_i\left(\frac{y}{a}\right) + \sum_{j=1}^{2} \varepsilon_m^j (d_1^j e^{B_j \frac{x}{a}} + d_2^j e^{B_j \frac{y}{a}} + d_3^j e^{-B_j \frac{x}{a}} + d_4^j e^{-B_j \frac{y}{a}}), \quad (23)$$

$$\hat{\Phi}_m(z) \approx c_{m,0}^{z} h_0 + \sum_{i=1}^{2} c_{m,i}^{z} h_i\left(\frac{z}{a_z}\right) + \sum_{j=1}^{2} \varepsilon_m^{z,j} \left(d_1^{z,j} e^{B_j^z \frac{z}{a_z}} + d_2^{z,j} e^{-B_j^z \frac{z}{a_z}} \right), \quad (24)$$

for $m = 0$ and $m = 2$. The following polynomials h_i of order i are chosen

$$h_0 = 1, \quad h_1(p) = 2\sqrt{3}p \quad \text{and} \quad h_2(p) = 6\sqrt{5}(p^2 - \frac{1}{12}). \quad (25)$$

The exponential functions in the expansion (23) and (24) are the solutions of the coupled homogeneous equations of (17) and (19) respectively. A quadratic equation system is obtained for the B_j^2 which results in two positive roots B_1^2, B_2^2. The same holds for the $(B_j^z)^2$. With $\varepsilon_0^j = \varepsilon_0^{z,j} = 1$ ($j = 1,2$), the other components of the corresponding eigenvector are given by

$$\varepsilon_2^j = \frac{\Sigma_{r,0} - D_0 B_j^2}{2\Sigma_{r,0}} \quad \text{and} \quad \varepsilon_2^{z,j} = \frac{\Sigma_{r,0} - D_0 (B_j^z)^2}{2\Sigma_{r,0}}. \quad (26)$$

for $j = 1$ and $j = 2$. The source and leakage terms $\hat{S}_0(x,y)$ and $L_m^{tr}(x,y)$ are only approximated by linear combinations of the polynomials h_0, $h_i(x)$ and $h_i(y)$ of (25), $\hat{S}_0(z)$ and $L_m^{tr}(z)$ accordingly by h_0 and $h_i(z)$, with $i = 1$ and $i = 2$. For simplification, $c_{m,i}^{x}$ and $c_{m,i}^{y}$ are called the coefficients c and $c_{m,0}^{z}$ and $c_{m,i}^{z}$ the coefficients c^z. Inserting the flux expansions into the equations (17) and (19) yields algebraic equation systems for the coefficients c and c^z. The coefficients d_1^j, d_2^j, d_3^j, d_4^j and $d_1^{z,j}$ and $d_2^{z,j}$ can be eliminated by the incoming partial currents and the coefficients c and c^z. From that fact, the outgoing partial currents are expressed by the incoming partial currents and the coefficients c and c^z, respectively.

An inner and outer iteration scheme is applied to solve the system of algebraic equations and to calculate the expansion coefficients and the node averaged fluxes for all nodes of the core. In the inner iteration, it is assumed that the polynomial coefficients of the fission and scattering sources and of the leakage are given from the last outer iteration. Based on these coefficients, the polynomial coefficients c and c^z are obtained from equation (17) and (19). Using these coefficients the outgoing partial currents are calculated for each node from the given incoming currents. The incoming currents are determined from the outgoing currents of the neighboring nodes using the interface conditions between the nodes or the boundary conditions at the core border.

After few (3 - 5) inner iterations the polynomial coefficients of the source terms are updated from the flux expansions (23) and (24) by weighting with the polynomials h_i in (25). The new coefficients of the source and leakage terms are used for the next outer iteration step. A Chebychev extrapolation scheme is applied to accelerate the outer iteration.

2.3. Application of the transport cross section in the SP_3 equations

In contrast to equation (4) first-order anisotropic group to group scattering will now be considered by using the so-called transport cross section, which is commonly used when the diffusion approximation is applied instead of the P_1 equations. Bell and Glasstone [8] consider the two P_1 equations for continuous energy and one-dimensional geometry. In order to approximately describe the two P_1 equations with the diffusion equation, they derive a reasonable expression for the diffusion coefficient $D(x,E)$. They use the approximation

$$\int \Sigma_{s,1}(x, E' \to E)\Phi_1(x, E')\, dE' \approx \int \Sigma_{s,1}(x, E \to E')\Phi_1(x, E)\, dE' , \tag{27}$$

where $\Sigma_{s,1}(x, E \to E')$ is the first moment of the macroscopic cross section for neutrons scattering from energy E to energy E' and $\Phi_1(x, E)$ the first flux moment at energy E. This approach is based on the argument that in the slowing down region the contribution on the left hand side of equation (27) comes from energies $E' > E$. It is nearly the same as the slowing down from energy E to lower energies. The right hand side can be described as

$$\int \Sigma_{s,1}(x, E \to E')\Phi_1(x, E)\, dE' = \Sigma_{s,0}(x, E)\overline{\mu}(x, E)\Phi_1(x, E) , \tag{28}$$

where $\Sigma_{s,0}(x, E)$ is the macroscopic scattering cross section and $\overline{\mu}(x, E)$ the average cosine of the scattering angle. With the transport cross section defined by

$$\Sigma_{tr}(x, E) \equiv \Sigma_t(x, E) - \int \Sigma_{s,1}(x, E \to E')\, dE' = \Sigma_t(x, E) - \overline{\mu}(x, E)\Sigma_{s,0}(x, E) , \tag{29}$$

the diffusion coefficient

$$D(x, E) = \frac{1}{3\Sigma_{tr}(x, E)} \tag{30}$$

is obtained. Thus, diffusion theory represents a form of the P_1 approximation in which the contribution of the anisotropic scattering to the energy transfer has been approximated by equation (27). Stamm'ler and Abbate [9] state that equation (27) is a good approximation if there is weak absorption.

For the multigroup equation system (3) with spatially constant cross sections in the nodes *n*, it follows from approximation (27) for the first-order group cross sections and flux moments

$$\sum_{g'=1}^{G} \Sigma^n_{s,1,g' \to g}\Phi^n_{1,g'}(x) \approx \sum_{g'=1}^{G} \Sigma^n_{s,1,g \to g'}\Phi^n_{1,g}(x) . \tag{31}$$

The corresponding transport cross section for interval *n* and energy group *g* is given by

$$\Sigma^n_{tr,g} = \Sigma^n_{t,g} - \sum_{g'=1}^{G} \Sigma^n_{s,1,g \to g'} . \tag{32}$$

Using approximation (31) and the transport cross section from (32) in the 2nd equation of (3) yields in the same manner the SP_3 equations (9) and (10), but with the diffusion coefficient

$$\widetilde{D}_{0,g}^{n} = \frac{1}{3\Sigma_{tr,g}^{n}} \tag{33}$$

instead of $D_{0,g}^{n}$ from the first equation of (8). The effect of the different approximations $D_{0,g}^{n}$ and $\widetilde{D}_{0,g}^{n}$ of the diffusion coefficient in the SP_3 equations on the results is investigated in the next section.

3. NUMERICAL RESULTS AND COMPARISONS

A steady state of the OECD/NEA and U.S. NRC PWR MOX/UO_2 Core Transient Benchmark [2] is used for verification of the SP_3 method in DYN3D. A simplified 3D core geometry was adopted for the benchmark purposes. The core has uniform fuel composition in axial direction and consists of 49 MOX fuel assemblies with 4.0 and 4.3 % Pu-fissile and 144 UO_2 assemblies with enrichments of 4.2 and 4.5 %. The burnup of the assemblies is different, but uniform in the axial direction. Fixed thermo-hydraulic conditions which correspond to hot zero power are given. Reflecting boundary conditions were considered at top and bottom core which makes the problem a two-dimensional one. In the calculation, the core is surrounded by assemblies describing the radial reflector with a baffle layer and a water reflector. The outer radial boundary condition is zero flux. All control rods are out of core. A 45 degree sector is considered because the core has a 45 degree reflectional (90 degree rotational) symmetry (see Fig. 1). The different colors refer to fresh, once and twice burnt fuel. Fig. 2 shows the configurations for the UO_2 and MOX fuel assemblies, which consists of 17×17 pins.

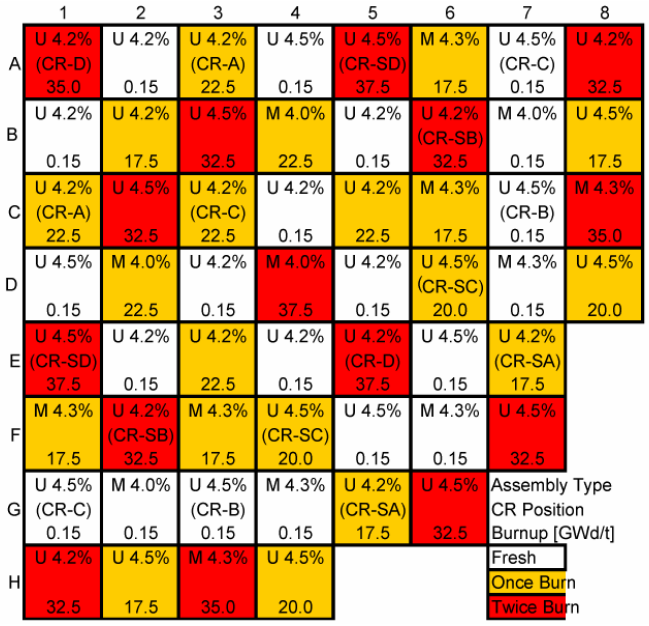

Figure 1. Core configuration of the PWR MOX/UO_2 benchmark.

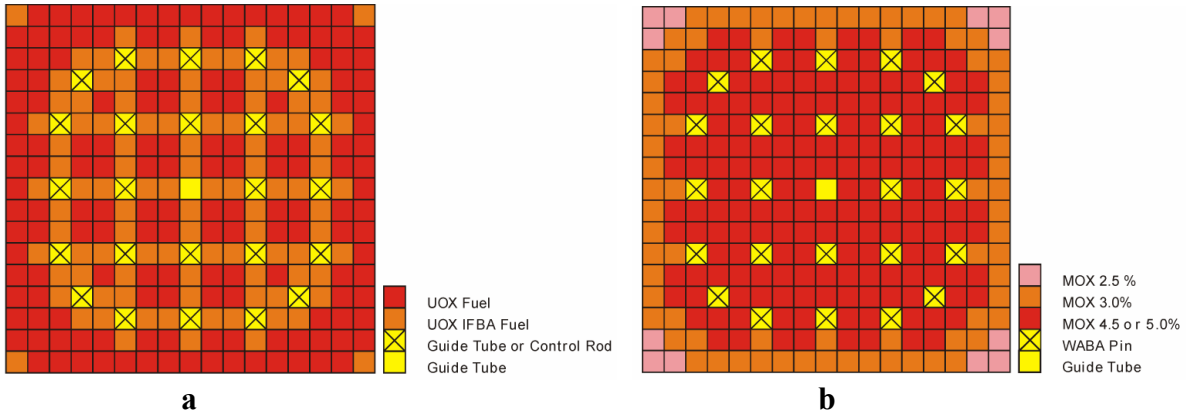

Figure 2. Structure of the UO_2 assembly (a) and the MOX assembly (b)

The DYN3D calculations were performed with one node per pin and a 16-group XS-library of pinwise homogenized cross sections, which was generated by the Gesellschaft fuer Anlagen- und Reaktorsicherheit (GRS) mbH with the cell code HELIOS 1.8 [5] for calculations with the transport code DORT [4]. HELIOS 1.8 yields only P_N data up to the order N = 1. Therefore, it is assumed $\Sigma^n_{s,l,g'\to g} = 0$ for $l = 2$ and $l = 3$ what results in $\Sigma^n_{r,2,g} = \Sigma^n_{r,3,g} = \Sigma^n_{t,g}$ in equation (6). The transport cross sections of (32) and the P_1 scattering moments are available in the library. For the baffle the P_1 scattering moments were used from the code RESMOD, because there are no P_1 data for iron within this HELIOS-version.

A solution generated with the code DeCART [3] is considered as reference. The method of characteristics was used for the solution of the neutron transport equation in DeCART. The heterogeneous structure of the pin cells is modeled. A 47-group library based on HELIOS version 1.8 with transport corrected P_0 scattering and subgroup methods for the resonance region was used. The DORT calculations performed by the GRS [4] are based on homogenized pin cells, 2×2 meshes per cell and the S_4 approximation.

The 16-group DORT library was used for three different DYN3D calculations. Firstly, a diffusion calculation DYN3D-DIFF was carried out with the diffusion coefficient defined by (33) with the group transport cross section from equation (32). The SP_3 calculation DYN3D-SP3-REM, in which the "removal" cross section $\Sigma^n_{r,1,g}$ from equation (6) is used to describe the diffusion coefficient $D^n_{0,g}$ from the first equation of (8), shows an accuracy which is not sufficient. The DYN3D-SP3-TR calculation is performed with the SP_3 method and the same diffusion coefficient of equation (33) as used in the DYN3D-DIFF calculation. Table I shows the results of the eigenvalues k_{eff} of the three DYN3D calculations and the DORT and MCNP results of [4] compared with the reference solution of the multigroup transport code DeCART. The DORT solution is based on the same cross section data for the homogenized pins.

The DYN3D-SP3-REM solution gives the highest deviation of k_{eff} in comparison to the DeCART and DORT results. The DYN3D-DIFF and the DYN3D-SP3-TR results show a good agreement with k_{eff} of the transport calculations. The comparisons of the DYN3D-SP3-REM

Table I. Eigenvalues k_{eff} and the RMS of the relative deviations (in %) of the assembly powers compared to the DeCART results.

Code	k_{eff}	RMS ass. powers
DeCart (Ref.)	1.05852	-
DYN3D-DIFF	1.05910	2.00
DYN3D-SP3-REM	1.06216	5.72
DYN3D-SP3-TR	1.05916	0.87
DORT	1.06036	0.95
MCNP	1.06065±0.00005	-

assembly powers in Fig. 3 show a maximum deviation from the DeCART solution of −9.17 %. The maximum deviation of the other two pinwise DYN3D calculations is given in the assembly no. 30 situated at the boundary of the core. It amounts to −3.85 % for the diffusion calculation DYN3D-DIFF and −1.86 % for the SP_3 calculation DYN3D-SP3-TR.

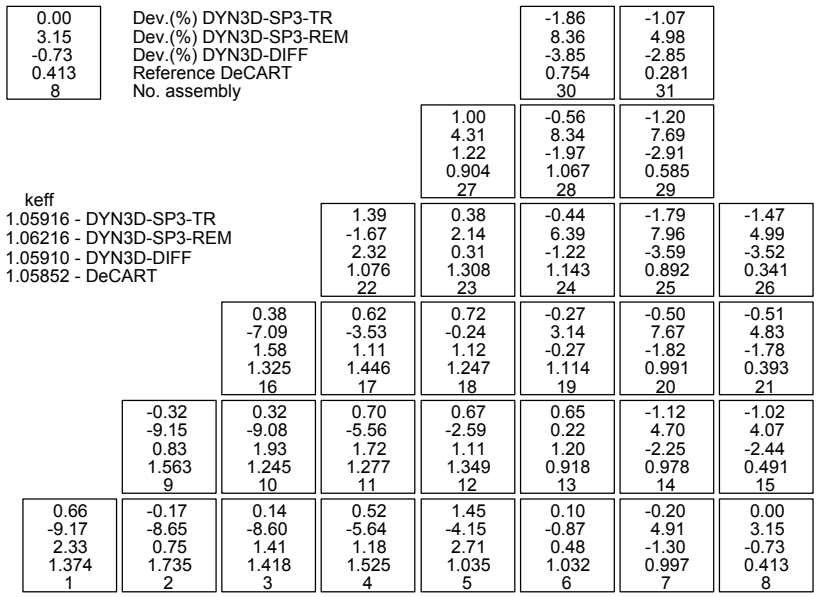

Figure 3. Comparison of the assembly powers of the three DYN3D calculations with the DeCART reference solution.

The RMS values of the comparisons of the assembly powers can be seen in Table I. They are in the same order for the DYN3D-SP3-TR and the DORT calculation. The results of DYN3D-SP3-TR with the RMS value of 0.87 % are much better than the DYN3D-SP3-REM results and better than the diffusion calculation. The application of the removal cross sections (6) with the approximation (4) in the SP_3 equations gives larger deviations than the diffusion theory. The solution is too flat, caused by the small values of the diffusion coefficients $D^n_{0,g}$ of equation (8) obtained by the approximation (4) and (6). The SP_3 theory with the usual diffusion coefficients

$\widetilde{D}^n_{0,g}$ from equation (33) instead of the coefficients $D^n_{0,g}$ provides a good agreement with the transport solution and shows also an improvement compared to the diffusion calculation.

The comparisons of the DYN3D results with the DORT solution in Fig. 4 show slightly larger deviations than the comparisons with the DeCART results in Fig. 3.

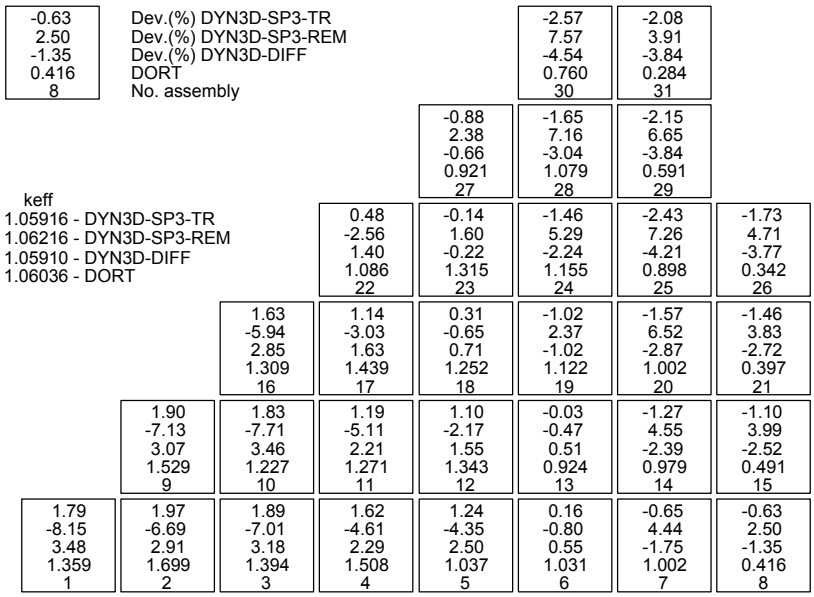

Figure 4. Comparison of the assembly powers of the DYN3D with the DORT results.

The pin powers of the DeCART solution are available for the diagonal row (assemblies 1, 9, 16, 22, 27, and 30 of Fig. 3). Fig. 5 shows the relative deviations between the DYN3D-SP3-TR and the DeCART results of the assembly-normalized pin powers for assembly 1 and 30. The powers of the 4 Integral Fuel Burnable Absorber (IFBA) pins of UO_2 assembly 1, which are the direct neighbors of the central guide tube pin cell in Fig. 2, show the highest deviation ($\delta = -2.18$ %).

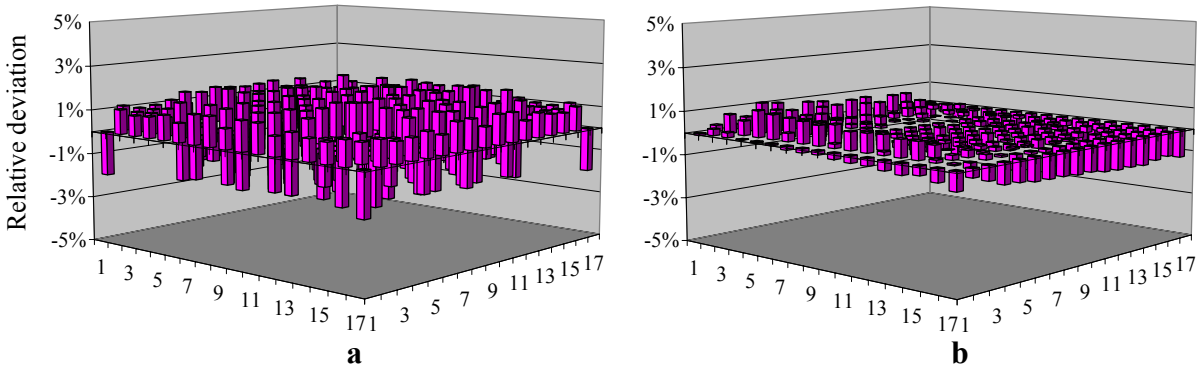

Figure 5. Comparison of the assembly-normalized pin powers of the DYN3D-SP3-TR and DeCART results for the central UO_2 assembly 1 (a) and peripheral MOX assembly 30 (b).

For the assemblies of the whole diagonal row Table II shows the maximum and the averaged (RMS) pin power deviations of the three DYN3D and the DORT results compared to DeCART. The maximum deviation of the DYN3D-SP3-TR result is given for the IFBA-fuel pin cell in the upper right corner of Fig. 2 for the UO_2 assembly no. 27 ($\delta = -2.79$ %). The comparisons of the DYN3D-SP3-REM and DYN3D-DIFF solutions show slightly higher deviations.

Table II. Maximum and RMS of the relative deviations (in %) of the assembly-normalized pin powers compared to the DeCART results for the assemblies in the diagonal row.

	DYN3D- SP3-TR		DYN3D- SP3-REM		DYN3D-DIFF		DORT	
Ass.	Max.	RMS	Max.	RMS	Max.	RMS	Max.	RMS
1	–2.18	1.58	–2.94	1.67	–2.55	1.60	–2.19	1.57
9	–1.12	0.66	–1.91	0.84	–1.00	0.64	1.19	0.64
16	–1.69	0.96	–4.19	1.84	–1.53	0.93	–2.17	1.01
22	–0.76	0.33	3.17	1.26	1.02	0.43	0.91	0.40
27	–2.79	1.71	–4.83	2.35	–4.28	1.79	–2.64	1.70
30	–1.30	0.58	–4.94	1.13	2.36	0.80	–1.43	0.53

Concerning the comparisons of the whole-core normalized pin powers the deviations of the assembly powers have to be considered too. As an example, Fig. 6 shows the relative deviations of the core-normalized pin powers of the DYN3D-SP3-TR and DYN3D-DIFF results compared to DeCART for the central assembly no. 1. The highest deviation is 2.58 % for the DYN3D-SP3-TR and 4.38 % for the diffusion calculation. This means, the more accurate results are the consequence of the improved assembly power distribution. Therefore, in general the DYN3D-SP3-TR results of the three DYN3D calculations show the lowest deviations from the DeCART solution. The deviations of the DORT results from the DeCART solution are in the same order.

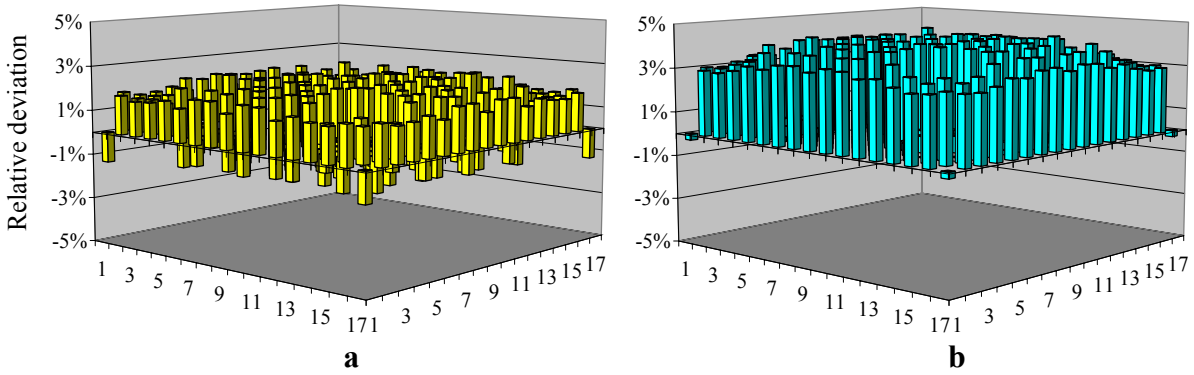

Figure 6. Comparison of the core-normalized pin powers of the DYN3D-SP3-TR (a) and the DYN3D-DIFF results (b) compared to DeCART for the central assembly no. 1.

It is interesting to analyze the effect of the second flux moment $\Phi_{2,g}$ on the results. If $\Phi_{2,g} = 0$, the first equation of (12) is equal to the diffusion equation for the scalar flux $\Phi_{0,g}$. Thus, the diffusion equation should be a good approximation, if the ratio $\Phi_{2,g}/\Phi_{0,g}$ is small. $\Phi_{2,g}/\Phi_{0,g}$ for the $9\times17 = 153$ pin cells of the central row of assembly no. 1 to 8 in Fig. 3 and the adjacent reflector assembly can be seen in Fig. 7 for the energy groups g = 1-5 and 12-16. The corresponding ratios for the groups 6-11 are not represented, because they are smaller and show no other significant characteristics. Only for the groups 1-4 (67.379 keV - 20 MeV) and 16 (10^{-4} eV - 0.056922 eV) and only in the reflector assembly and the adjacent UO_2 assembly no. 8 the amount of $\Phi_{2,g}/\Phi_{0,g}$ has values greater than 0.05. Fig. 7a shows for the fast groups that $\Phi_{2,g}/\Phi_{0,g}$ increases in the transition from the UO_2 assembly no. 8 to the reflector assembly. In the reflector $\Phi_{2,g}/\Phi_{0,g}$ is noticeably higher than in the fuel. This means, that for fast neutrons the dependence of the angular flux on the neutron direction is greater in the reflector than in the fuel region of the core. This dependence increases with higher neutron energy. For the slow neutrons, Fig. 7b shows a peak at pin cell no. 137 and 138 which are just the two pin cells of the reflector assembly with the baffle material. Thus, in the baffle the dependence of the angular flux on the neutron direction increases with decreasing neutron energy. Fig. 7 also illustrates the small positive and negative peaks in each fuel assembly at the 5 guide tube or Wet Annular Burnable Absorber (WABA) pins of the central row (see Fig. 2). The amount of $\Phi_{2,g}/\Phi_{0,g}$ is almost always lower than 0.02 for the pin cells in the fuel assemblies. Only for the central guide tube pin cell no. 94 of the MOX assembly no. 6 and the pin cells no. 134 to 136 of the UO_2 assembly no. 8 near the baffle the ratio $\Phi_{2,g}/\Phi_{0,g}$ reaches values up to 0.041 for some energy groups.

In contrast to the change of $\Phi_{2,g}/\Phi_{0,g}$ at the transition from the reflector to the fuel, the change of this ratio is not significant inside the core. This suggests to solve the both SP_3 equations (12) not always in parallel, but in some assemblies and for certain iteration steps the second after the first.

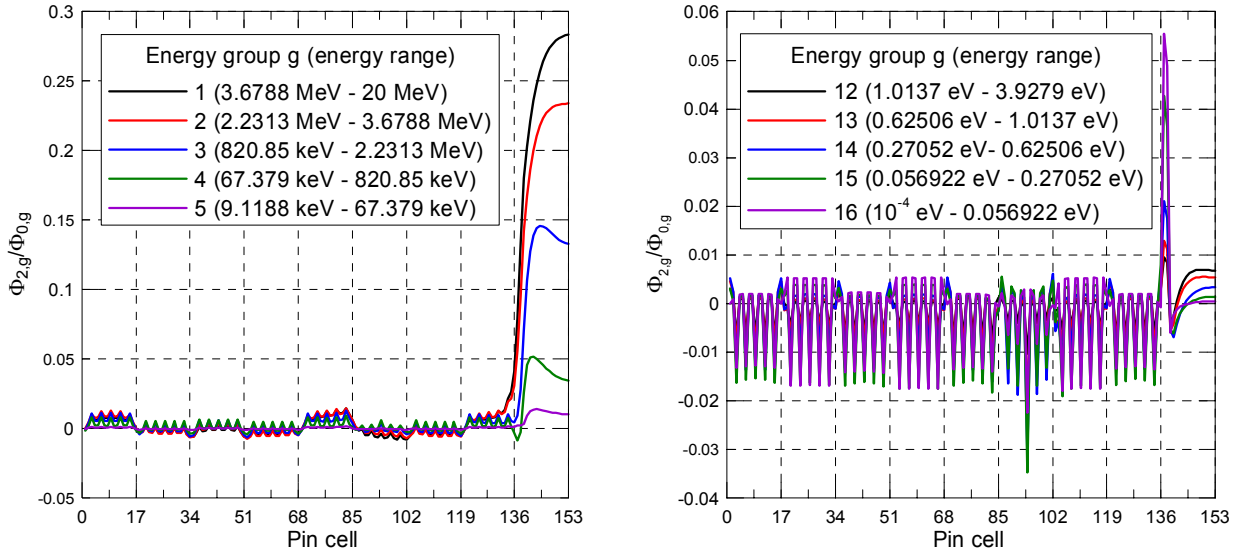

Figure 7. $\Phi_{2,g}/\Phi_{0,g}$ for the 153 pin cells of the central pin cell row of assembly 1 to 8 and the adjacent reflector assembly for energy group g = 1 – 5 (a) and g = 12 – 16 (b)

4. CONCLUSION AND OUTLOOK

A multigroup SP_3 method was presented and implemented in the reactor core model DYN3D. The results of pinwise calculations were compared with the results of the transport codes DeCART and DORT for a steady state of the OECD/NEA and U.S. NRC PWR MOX/UO_2 Core Transient Benchmark. Using the transport cross section of diffusion theory in the SP_3 method the DYN3D-SP3 results show a very good agreement with the reference DeCART solution. The deviations are in the order of those between the DeCART and the DORT results. The SP_3 method shows also an obvious improvement compared to the diffusion solution. Since the ratio $\Phi_{2,g}/\Phi_{0,g}$ of the 2^{nd} to the 0^{th} flux moment is small inside the core for each energy group *g* alternative simpler algorithms are included in DYN3D-SP3. It is encouraging to develop the method for standard applications in core calculations including the simulation of transients. Further verifications are necessary, especially for cores with MOX loadings and inserted control rods.

ACKNOWLEDGMENTS

This work is funded by the German Federal Ministry of Economics and Labor. The authors thank A. Seubert of the Gesellschaft fuer Anlagen- und Reaktorsicherheit (GRS) mbH for providing the library of group constants and the results calculated with the code DORT.

REFERENCES

1. U. Grundmann, U. Rohde, S. Mittag, “DYN3D – Three Dimensional Core Model for Steady-State and Transient Analysis of Thermal Reactors”, *Proc. of the 2000 ANS International Topical Meeting on Advances in Reactor Physics and Mathematics and Computation into the Next Millennium (PHYSOR 2000)*, Pittsburgh (USA), May 7-11 (2000).
2. T. Kozlowski, T. J. Downar, “OECD/NEA and U.S. NRC PWR MOX/UO_2 Core Transient Benchmark”, Working Party of the Physics of Plutonium Fuels and Innovative Fuel Cycles, OECD/NEA Nuclear Science Committee (2003).
3. H. G. Joo, J. Y. Cho, Y. Kim “Dynamic Implementation of the Equivalence Theory in the Heterogeneous Whole Core Transport Calculation”, *Proceedings of PHYSOR 2002 International Conference on the New Frontiers of Nuclear Technology: Reactor Physics, Safety and High-Performance Computing*, Seoul, Korea, Oct. 7-10 (2002).
4. A. Seubert, S. Langenbuch, W. Zwermann, “Solution of the Stationary State of the PWR MOX/UO_2 Core Transient Benchmark”, *Proc. of PHYSOR-2006, ANS Topical Meeting on Reactor Physics*, Vancouver, BC, Canada, September 10-14 (2006).
5. Studsvik® Scandpower, “HELIOS Methods, Version 1.8”, Studsvik Scandpower, November 20 (2003).
6. P. S. Brantley, E. W. Larsen, “The Simplified P_3 Approximation”, *Nucl. Sci. Eng.*, **134**, pp.1-21 (2000).
7. E. M. Gelbard, “Application of Spherical Harmonics Methods to Reactor Problems”, WAPD-BT-20, Bettis Atomic Power Laboratory (1960).
8. G. I. Bell, S. Glasstone, *Nuclear Reactor Theory*, Van Nostrand Reinhold Company, New York (1970).
9. R. J. J. Stamm’ler, M. J. Abbate, *Methods of Steady-State Reactor Physics in Nuclear Design*, Academic Press Inc., London (1983).